Atmos. Chem. Phys. Discuss., https://doi.org/10.5194/acp-2017-584
Manuscript under review for journal Atmos. Chem. Phys.
Discussion started: 27 June 2017

Atmospheric Chemistry and Physics Discussions

Characterization of organic nitrate constituents of secondary organic aerosol (SOA) from nitrate-radical-initiated oxidation of limonene using High-Resolution Chemical Ionization Mass Spectrometry

Cameron Faxon[1], Julia Hammes[1], Ravi Kant Pathak[1], Mattias Hallquist[1]

[1]Department of Chemistry and Molecular biology, University of Gothenburg, Göteborg, SE-41258, Sweden

Abstract: The gas phase nitrate radical ($NO_3^•$) initiated oxidation of limonene can produce organic nitrate species with varying physical properties. Low-volatility products can contribute to secondary organic aerosol (SOA) formation and organic nitrates may serve as a NO_x reservoir, which could be especially important in regions with high biogenic emissions. This work presents the measurement results from flow reactor studies on the reaction of $NO_3^•$ and limonene using a High-Resolution Time-of-Flight Chemical Ionization Mass Spectrometer (HR-ToF-CIMS) combined with a Filter Inlet for Gases and AEROsols (FIGAERO). Major condensed-phase species were identified, and the identity and volatility properties of the most prevalent organic nitrates in the produced SOA were determined. Analysis of multiple experiments resulted in the identification of several dominant species (including $C_{10}H_{15}NO_6$, $C_{10}H_{17}NO_6$, $C_8H_{11}NO_6$, $C_{10}H_{17}NO_7$, and $C_9H_{13}NO_7$) that occurred in the SOA under all conditions considered. The observed and expected (listed) products (associated with the Master Chemical Mechanism (MCM) limonene mechanism) were compared, and many non-listed species were identified. Additionally, the formation of dimers was consistently observed and these species resided almost completely in the particle phase. The identities of these species are discussed, and formation mechanisms are proposed. Cluster analysis of the desorption temperatures corresponding to the analyzed particle-phase species yielded at least five distinct groupings based on a combination of molecular weight and desorption profile. Overall, the results indicate that the oxidation of limonene by $NO_3^•$ produces a complex mixture of highly oxygenated monomer and dimer products that contribute to SOA formation.

1 Introduction

Oxidation of gas-phase organic species contribute significantly to particle formation and growth (Hallquist et al., 2009; Smith et al., 2008; Wehner et al., 2005), and thus a thorough understanding of secondary organic aerosol (SOA) formation mechanisms is important for the accurate estimation of its impact on the climate system (Kanakidou et al., 2005).

Secondary organic aerosols form primarily via the photooxidation of volatile organic compounds (VOCs), yielding less volatile products, which can then partition into the condensed phase (Hallquist et al., 2009; Kroll and Seinfeld, 2008), especially when pre-existing aerosols (e.g., inorganic seed particles) are present (Kroll et al., 2007). The products resulting from atmospheric oxidation may be classified as low volatility, semi-volatile, and intermediate volatility OCs, i.e.,

Atmos. Chem. Phys. Discuss., https://doi.org/10.5194/acp-2017-584
Manuscript under review for journal Atmos. Chem. Phys.
Discussion started: 27 June 2017

Atmospheric Chemistry and Physics Discussions

LVOCs, SVOCs, and IVOCs, respectively (Donahue et al., 2012; Jimenez et al., 2006; Murphy et al., 2014). In addition, extremely low volatility OCs (i.e., ELVOCs) contribute significantly to aerosol formation and early growth (Ehn et al., 2014; Jokinen et al., 2015). The photo-oxidation of VOCs by the primary atmospheric oxidants, O_3 and $^{\bullet}OH$, has been extensively investigated (Cao and Jang, 2008; Hallquist et al., 2009; Kanakidou et al., 2005; Kroll and Seinfeld, 2008). Although less studied than the photo-oxidation of VOCs, the reaction of VOCs with the nitrate radical ($NO_3^{\bullet}$) and the resulting formation of organic nitrates are also important, especially for nocturnal chemistry (Brown and Stutz, 2012; Perring et al., 2013; Roberts, 1990). Significant concentrations of these nitrates have been detected in the gas and condensed phases in both field and laboratory studies (Ayres et al., 2015; Beaver et al., 2012; Bruns et al., 2010; Lee et al., 2016; Paulot et al., 2009; Rindelaub et al., 2014, 2015, Rollins et al., 2012, 2013).

Organic nitrates ($RONO_2$) and organic peroxy nitrates (RO_2NO_2), such as peroxy acetyl nitrate (PAN), may also form in the atmosphere (Roberts, 1990; Singh and Hanst, 1981; Temple and Taylor, 1983). RO_2NO_2 may form via the reaction of organic peroxy nitrates ($RO_2^{\bullet}$) with NO_2, while $RONO_2$ may form directly through either the reaction of $RO_2^{\bullet}$ with NO or the reaction of unsaturated VOCs with $NO_3^{\bullet}$. Reactions 1–2 show the typical formation pathway of organic nitrates and peroxy nitrates formed from the reactions of NO_x with $RO_2^{\bullet}$ originating from a generic VOC, R

$$RO_2^{\cdot} + NO \xrightarrow{(a)} NO_2 + RO^{\cdot} \quad \text{(R1a)}$$

$$\xrightarrow{(b)} RONO_2 \quad \text{(R1b)}$$

$$RO_2^{\cdot} + NO_2 \longrightarrow RO_2NO_2 \quad \text{(R2)}$$

Secondary organic aerosol-precursor VOCs arise mainly from the emission and reaction of biogenic VOCs (BVOCs) (M. Hallquist et al., 2009), with up to 90% of the global VOC budget originating from biogenic sources (Glasius and Goldstein, 2016; Guenther et al., 1995). Isoprene, the main constituent of global BVOC terrestrial emissions (600 Tg yr^{-1}) (Guenther et al., 2006), is highly reactive with $^{\bullet}OH$, O_3, and $NO_3^{\bullet}$ (Atkinson et al., 1995; Hallquist et al., 2009). However, monoterpenes typically have higher SOA yields than isoprene (Carlton et al., 2009; Presto et al., 2005b) and regarding atmospheric emissions, α-pinene, β-pinene, and limonene constitute the main monoterpenes emitted into the atmosphere (Guenther et al., 2012). In addition to its high emission rates, limonene is especially interesting as a model BVOC, due to its relatively high reaction rates (Ziemann and Atkinson, 2012) and occurrence in indoor environments, owing to emission sources, such as air fresheners and other household products (Wainman et al., 2000).

The reactions and mechanisms of α-pinene and β-pinene oxidation have been more thoroughly studied (Bonn and Moorgat, 2002; Fry et al., 2009; Perraud et al., 2010; Presto et al., 2005a, 2005b) than those associated with limonene. Several studies have focused on the ozonolysis of and SOA formation from limonene (Baptista et al., 2011; Jiang et al., 2013; Jonsson et al., 2006, 2008a; Leungsakul et al., 2005; Pathak et al., 2012; Sun et al., 2011;

Atmos. Chem. Phys. Discuss., https://doi.org/10.5194/acp-2017-584
Manuscript under review for journal Atmos. Chem. Phys.
Discussion started: 27 June 2017

Atmospheric Chemistry and Physics Discussions

Youssefi and Waring, 2014; Zhang et al., 2006). $NO_3^{\bullet}$ oxidation of limonene and the resulting organic nitrates that may contribute to SOA formation have, however, rarely been investigated (Fry et al., 2011, 2014; Hallquist et al., 1999; Spittler et al., 2006). In relation to the reaction with $NO_3^{\bullet}$, major non-nitrate products of limonene (including endolim) have been identified, but significant SOA formation was preceded by the occurrence of multiple unidentified nitrates (Hallquist et al., 1999; Spittler et al., 2006). Moreover, although mechanistic models and molecular identities of these products have been proposed, direct measurement and identification thereof have yet to be reported. Further elucidation of the mechanisms governing and products generated by the reactions of limonene and $NO_3^{\bullet}$ are warranted, since organic nitrates from BVOCs (including limonene) have been consistently observed in field studies (Ayres et al., 2015; Beaver et al., 2012; Lee et al., 2016, 2014b; Perring et al., 2009).

Additionally, the contribution of low-volatility products to the SOA mass may increase with the formation of dimers from aerosol components generated by VOC oxidation. Numerous dimers or oligomers have been found in SOA generated by monoterpene species (e.g. Emanuelsson et al., 2013; Kourtchev et al., 2014, 2016; Kristensen et al., 2016; Müller et al., 2007; Tolocka et al., 2004). However, the speciation of observed dimers and oligomers from organic nitrates, especially with respect to detailed formation mechanisms, has rarely been reported.

Here we report the chemical composition of low-volatility gas and aerosol-phase species, formed from mixtures of N_2O_5 and limonene, as measured by a High Resolution Time-of-Flight Chemical Ionization Mass Spectrometer (HR-ToF-CIMS) coupled to a Filter Inlet for Gases and AEROsols (FIGAERO) inlet (Lopez-Hilfiker et al., 2014). The objectives of this work were three-fold namely, to: (i) determine the molecular formula of major nitrate species, produced from the reaction of limonene with $NO_3^{\bullet}$, that could contribute significantly to SOA formation and growth, (ii) compare the distribution of measured products to that of the expected products (formed via the Master Chemical Mechanism (MCM)) to identify any discrepancies in the mechanistic understanding of nitrate formation from limonene, and (iii) categorize, via cluster analysis, the thermodynamic desorption data measured for selected condensed-phase species.

2 Methods

2.1 Experimental setup

Experiments were performed in the Gothenburg Flow Reactor for Oxidation Studies at low Temperatures (GFROST) at the University of Gothenburg. In previous studies, this facility was used for studying the impact of relative humidity, OH-scavengers, and temperature on SOA formation via monoterpene ozonolysis (Emanuelsson et al., 2013; Jonsson et al., 2008a, 2008b), its volatility properties (Pathak et al., 2012), and dimer formation during the ozonolysis of α-pinene (Kristensen et al., 2016). The inflow of zero air and the reagents is fixed at a total flow of 1.6 L per min (LPM). The experiments are all run at low RH (≤1%) and a constant temperature of 20°C. To catch only the center portion of the laminar flow and avoid unnecessary interference

Atmos. Chem. Phys. Discuss., https://doi.org/10.5194/acp-2017-584
Manuscript under review for journal Atmos. Chem. Phys.
Discussion started: 27 June 2017

Atmospheric Chemistry and Physics Discussions

from wall effects, samples are taken through a cone at the end of the reactor at 0.95 LPM. The average residence time of the sampled portion of the mixture is 240 s. Due to the flow restrictions, a make-up flow of zero air is added to the sample, immediately after the outlet, prior to being sampled by the instruments. The amount of dilution flow necessary is constrained by the flow required by the HR-ToF-CIMS. Figure 1 shows a diagram of the experimental setup.

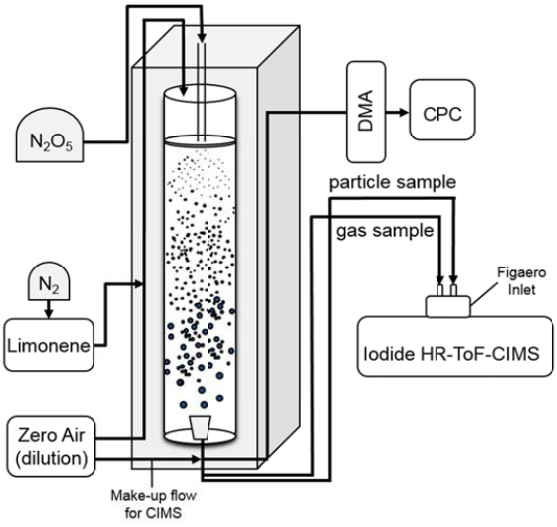

Figure 1. Diagram of experimental setup of GFROST during experiments.

Gas and particle-phase products were measured using a High-Resolution Time-of-Flight Chemical Ionization Mass Spectrometer (HR-ToF-CIMS) coupled to a Filter Inlet for Gases and AEROsols (FIGAERO) (Lopez-Hilfiker et al., 2014). The HR-ToF-CIMS can be operated in either negative- or positive-ionization modes, using various reagent-ion sources. CIMS measurement techniques have previously been employed for the measurement of organic nitrate products of monoterpenes (Beaver et al., 2012; Paulot et al., 2009) using multiple reagent ions (Lee et al., 2014a). In this work, the HR-ToF-CIMS was operated using negative Iodide (I^-) ion as the reagent in all experiments. Dry UHP N_2 was passed over a permeation tube containing liquid CH_3I (Alfa Aesar, 99%), and $I(H_2O)_n^-$ ions were generated by directing the flow over a ^{210}Po radioactive source. Reaction products (e.g., species X) were identified by their corresponding cluster ions, XI^-, thereby allowing the collection of whole-molecule data. The reagent and sample flowed into the Ion-Molecule Reaction (IMR) chamber of the instrument at a nominal individual rate of 2 LPM. The IMR was temperature-controlled at 40°C and operated at a nominal pressure of 200 mbar. With I^- ionization, the sensitivity of a detected species (i.e., hz ppt^{-1}) can vary significantly with relative humidity (Lee et al., 2014a). However, the experiments were all performed at low RH (≤1%) and, hence, the same sensitivity was realized for all the conditions considered.

Atmos. Chem. Phys. Discuss., https://doi.org/10.5194/acp-2017-584
Manuscript under review for journal Atmos. Chem. Phys.
Discussion started: 27 June 2017

Atmospheric Chemistry and Physics Discussions

The FIGAERO inlet was used during the experiments, and particles were collected on a Zefluor® PTFE membrane filter. The aerosol sample line and gas sample line were composed of 12 mm copper tubing and 12 mm Teflon tubing, respectively. The inlet was operated in regular cycles – 1 h of gas-phase sampling and simultaneous particle collection, followed by a 1-h period where the filter was shifted into position over the IMR inlet and the collected SOA was desorbed. Desorption was facilitated by a 2 LPM flow of heated UHP N_2 over the filter. The temperature of the N_2 was increased from 20 to 200°C in 50 min (3.5°C min^{-1}), and a subsequent 10-minute temperature soak was performed to ensure complete removal of the remaining organic material that volatilizes at 200°C. The measured species were distinguished based on their thermal properties via the resulting desorption time-series profiles, hereafter referred to as thermograms. Temperature gradients of >3.5°C min^{-1} have been used in previous studies, but, in this work, a lower gradient was used to enable optimum thermal separation (Lee et al., 2014a; Lopez-Hilfiker et al., 2014). The HR-ToF-CIMS was configured to measure singly charged ions with a mass-to-charge ratio (*m/z* or Th) of 7–720. Particles were contemporaneously sampled directly at the outlet of the flow reactor, through a ¼″ stainless steel 1 m sample line, by a Scanning Mobility Particle Sizer (SMPS). The SMPS measured the number-size distribution used for estimating the mass concentrations, based on the assumption of spherical particles with a density of 1.4 (Hallquist et al., 2009). In all cases, SOA was generated via nucleation and growth rather than by using seed particles.

2.2 Reagent preparation

N_2O_5 was synthesized by reacting ≥20 ppm O_3 with pure NO_2 (98%, AGA Gas) in a glass vessel and then passing the flow through a cold trap maintained at -78.5°C by dry ice. The resulting white solid showed signs of yellowing, due to nitric or nitrous acid contamination, only when exposed to moisture (e.g., ambient lab air). The solid N_2O_5 was transferred to a diffusion vial fitted with a capillary tube (inner diameter: 2 mm). The N_2O_5 diffusion source was held at a constant temperature (-23 °C), and the gravimetrically determined mass loss rate remained steady (r^2 value: 0.97–0.98) for several weeks. A similarly characterized d-limonene (Alfa Aesar, 97%) diffusion source was held at temperatures ranging from 8.5 to 31.5°C and, using Gas Chromatography–Mass Spectrometry (GC-MS; Finnigan/Tremetrics), diluted flow-reactor concentrations (15, 45, 92, and 150 ppb)..

Experiments were performed over a range (1.0–113) of N_2O_5/limonene ratios (see Table 1 for a summary of experimental conditions). For each set of conditions in the flow reactor, sampling was performed over a period of 6–12 h to ensure stability of conditions (e.g., gas-phase signals, total SOA mass) and repeatability of the FIGAERO thermal-desorption cycles.

Atmos. Chem. Phys. Discuss., https://doi.org/10.5194/acp-2017-584
Manuscript under review for journal Atmos. Chem. Phys.
Discussion started: 27 June 2017

Atmospheric Chemistry and Physics Discussions

173 **Table 1.** Experimental conditions considered in this study.

#	N_2O_5 (ppb)	Limonene (ppb)	N_2O_5 / Limonene	Average SOA Mass (μg m^3)
1	160	15	10.7	8.1
2	95	40	2.4	8
3	95	15	6.3	12
4	95	15	6.3	8
5	95	40	2.4	10
6	95	95	1.0	12
7	1700	15	113.3	7
8	1700	40	42.5	11
9	1700	95	17.9	43
10	1700	150	11.3	95
11	850	95	8.9	25
12	850	150	5.7	47

174

175 **2.3 CIMS data-analysis methods**

176 Data obtained from the HR-ToF-CIMS was analyzed using the Tofware
177 (Tofwerk/Aerodyne) analysis software written in Igor Pro (WaveMetrics). High-resolution
178 analysis allowed for ion identification with a resolution of ~4000 (m/Δm). Identified species were
179 cross-checked with predicted species generated via the MCM v3.3.1 limonene mechanism
180 (Saunders et al., 2003) and the corresponding theoretical product distribution was compared with
181 the measured distribution. For several ions, product formulas in the MCM were used as the major
182 parameter for ion identification at a given *m/z*. However, this identification scheme resulted in the
183 misidentification of several ions. The identification of high-mass ions (*m/z* > 500) was
184 complicated by the fact that the number of possible formulas increases rapidly with increasing
185 mass and carbon number of the ions. Nevertheless, the high accuracy of fits (≤5 ppm), where the
186 identities of expected product ions were corroborated by the fits of expected isotopes, reduced
187 uncertainties stemming from the mass calibration and provided reliable ion identifications. To
188 further ensure the accuracy of the identities of high-mass ions, the fits of the identified ions were
189 compared over all experiments.

190 The high-resolution ion data was further analyzed with Python 3.5.2 using the pandas
191 (McKinney, 2010, 2011) and NumPy (Van Der Walt et al., 2011) packages, and peaks in the ion
192 thermograms were identified using an implementation of the PeakUtils package (v1.0.3,
193 http://pythonhosted.org/PeakUtils/). For each experiment, the temperature (T_{max}) corresponding
194 to the peak signal of each ion observed during the desorption of SOA particles was identified.
195 Furthermore, a secondary temperature ($T_{max,2}$) was identified when double-peak behavior was
196 observed.

Atmos. Chem. Phys. Discuss., https://doi.org/10.5194/acp-2017-584
Manuscript under review for journal Atmos. Chem. Phys.
Discussion started: 27 June 2017

2.4 Cluster-analysis methods

Cluster analysis, performed via the K-Means algorithm (scikit-learn machine learning package; Pedregosa et al., 2011), was used to distinguish, based on their elemental composition and thermodynamic behavior (T_{max}), groups of ions observed during SOA desorption. This algorithm, utilizing a random seeding approach (Arthur and Vassilvitskii, 2007), was chosen due to the superior cluster separation realized after comparing several algorithms, including affinity propagation and mean-shift clustering. The solution of the K-Means algorithm is obtained through the minimization of an inertia function (see Eq. 1) Φ, which is equivalent to the sum of the mean-squared distance between all samples and their corresponding cluster centroid, c (Arthur and Vassilvitskii, 2007; Raschka, 2016). Here, $x^{(i)}$: sample (e.g., carbon number, oxygen number, T_{max}) in a set of n samples, $c^{(j)}$: cluster center of cluster j in a set of k clusters, and $w^{(i,j)}$: weighting coefficient ($w^{(i,j)} = 1$ if $x^{(i)}$ is in cluster j, $w^{(i,j)}=0$ otherwise).

$$\phi = \sum_{i=1}^{n}\sum_{j=1}^{k} w^{(i,j)}\left\|x^{(i)} - c^{(j)}\right\|^2 \quad (1)$$

The quality of the cluster separation was assessed through a silhouette score (Rousseeuw, 1987), which allows comparison of the intra-cluster and inter-cluster distances and, for a sample i, is determined from:

$$s(i) = \frac{b(i)-a(i)}{max\{a(i),b(i)\}} \quad (2)$$

where, a(i): average distance, or dissimilarity, between point i and each point within its own cluster and b(i): average dissimilarity between point i and all points within the nearest neighboring cluster. The value of s(i) ranges from -1 to 1 and reflects the quality of the clustering with respect to the separation between members of each cluster. For example, a score of ~1 indicates that the point is relatively far away from the nearest neighboring cluster, while a score of 0 suggests that the cluster separation is roughly equivalent to that of cohesion clusters; that is, $a(i) \approx b(i)$. For all points within a clustered dataset, an average silhouette score can indicate the adequacy of the cluster separation for a given number of clusters.

Detected ions were clustered based on their molecular weight (MW), elemental numbers (n_c, n_H, n_O, n_N), and T_{max} values. Compared with the other variables, MW and the carbon number exhibited the highest correlation with T_{max}. Clustering the ions based on these three variables yielded the best separation with respect to mass and T_{max} of the ions. Input variables were scaled to values between 0 and 1 (based on their respective range of input values) to prevent any bias associated with the relative magnitude of each variable (e.g., MW >> n_C).

Atmos. Chem. Phys. Discuss., https://doi.org/10.5194/acp-2017-584
Manuscript under review for journal Atmos. Chem. Phys.
Discussion started: 27 June 2017

Atmospheric Chemistry and Physics Discussions

3 Results and discussion

3.1 Characterization of mass spectra from SOA and identification of species

Products in both the gas and condensed phases were identified by analyzing HR-ToF-CIMS data collected under various experimental conditions (Table 1). In each sampling regime, major products were readily identifiable, and only modest or negligible fragmentation occurred with application of the soft ionization technique. The mass-to-charge (*m/z* or Th) values of the most prominent ions of species detected in the collected aerosol were determined from the average mass spectra obtained during desorption cycles. The results revealed two distinct regions consisting of several clusters of elevated ion signals (Fig. 2). These regions corresponded to aerosol samples considered in all experiments (Table 1), and the relative signal intensities varied with the amount of limonene and N_2O_5 present in the system. The occurrence of ions in these regions indicates a prevalence of lower-mass monomer species and higher-mass dimer species. These results are analogous to those of previous ozonolysis studies, where highly oxygenated multifunctional (HOM) molecules from monoterpene oxidation were observed using a nitrate HR-ToF-CIMS (Ehn et al., 2014; Jokinen et al., 2015; Mentel et al., 2015). Figure 2 shows an average mass spectrum corresponding to four sequential 1-h desorption cycles of 12-μg m^{-3} SOA samples from a reaction mixture with a N_2O_5 to limonene ratio of 2.4.

In total, 198 of the identified organic ions constituted significant fractions of the aerosol samples, but most of the signal emanated from only ~25% of these species. The dominant species were identified by averaging the desorption-time series of all experiments and extracting the top 75^{th} percentile (by averaging the signal during desorption) of the monomer and dimer ions. The resulting set of ions consisted of 52 molecular species that accounted for 76% of the organic signal during desorption, while the top 90^{th} percentile of ions (20 ions) accounted for 56%. This 52-ion set consisted of 28 monomers (C = 7–10) and 24 dimers or oligomers (C = 11–20). On average, the top 75^{th} percentile of monomers and the top 75^{th} percentile of dimers accounted for 83% of the total monomer signal and 70% of the total dimer signal, respectively. A full list of ions and the composition of the 40^{th}, 75^{th}, and 90^{th} percentile subsets can be found in the Supplementary Information.

The first, i.e., lower-mass region, of the two mass-spectra regions (see Fig. 2) occurred at *m/z* values ranging from 350 to 450. Several ions in this region matched the predicted molecular formulas associated with the MCM limonene mechanism, and the largest signals occurred for species consisting of 8–10 carbon atoms. E.g. the dominant ions occurring at *m/z* 360, 372, 374, and 390 (during desorption) corresponded to the iodide-cluster ions $C_8H_{11}NO_7I^-$, $C_{10}H_{15}NO_6I^-$, $C_{10}H_{17}NO_6I^-$, and $C_{10}H_{17}NO_7I^-$ (Fig. 2a). These correspond to the MCM species C727PAN and C731PAN, C923PAN, NLIMALOH and LIMALNO3, NLIMALOOH, respectively.

Atmos. Chem. Phys. Discuss., https://doi.org/10.5194/acp-2017-584
Manuscript under review for journal Atmos. Chem. Phys.
Discussion started: 27 June 2017

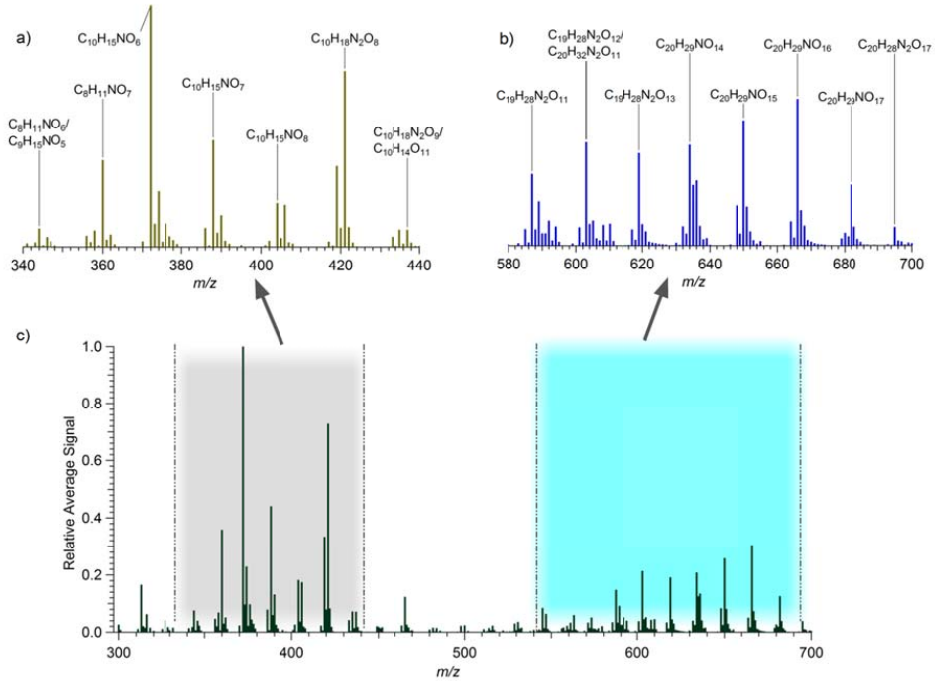

Figure 2. Representative average mass spectrum for the desorption of SOA collected during the experiments: Identification of ions detected in the (a) monomer region (*m/z* 340–440) and (b) dimer region (*m/z* 580–700). (c) Relative intensities and positions of the two regions detected in all aerosol samples. Data was obtained from four 1-h desorption cycles of 12-µg m^{-3} samples from a mixture with a N_2O_5/limonene ratio of 2.4. The un-clustered (i.e., not clustered with I⁻) *m/z* of each ion is –127 *m/z*.

Elevated signals of monomer ions (e.g., $C_{10}H_{15}NO_7$ (*m/z* 388), $C_{10}H_{15}NO_8$ (*m/z* 404), $C_{10}H_{17}NO_8$ (*m/z* 406), and $C_{10}H_{15}NO_9$ (*m/z* 420)), which are absent from the list of expected products of the mechanism, also occurred in this region. These non-MCM species contributed, at least modestly, to the total organic monomer signal, and MCM species accounted for only 43.5 ± 3.2% of the total monomer signal of all experiments. In contrast to the MCM species, the monomers contain one nitrogen atom and more than six oxygen atoms.

Monomers with progressively more oxygenated species of the general formula $C_{10}H_{15}NO_x$ were detected for x = 5–9 (i.e., $C_{10}H_{15}NO_5$–$C_{10}H_{15}NO_9$) with $C_{10}H_{15}NO_6$ being the dominant species in both the aerosol and gas phase in most experiments. Ions with molecular formulas containing two nitrogen atoms, for example, $C_{10}H_{16}N_2O_8$ (*m/z* 419) and $C_{10}H_{18}N_2O_8$ (*m/z* 421), were also detected (Fig. 2a). Limonene and its primary products reacted only with NO_2, $NO_3^{\bullet}$, and HNO_3, yielding molecules that are most likely di-nitrate species, with additional functional groups. Some of the measured species could either be peroxy nitrates or similar in structure to peroxy acetyl nitrate (PAN). PAN-like species readily undergo thermal degradation

Atmos. Chem. Phys. Discuss., https://doi.org/10.5194/acp-2017-584
Manuscript under review for journal Atmos. Chem. Phys.
Discussion started: 27 June 2017

Atmospheric Chemistry and Physics Discussions

(Orlando et al., 1992; Tuazon et al., 1991; Wooldridge et al., 2010) at temperatures significantly lower than those (100–200°C) used to heat the samples. Therefore, the number of intact PAN-like ions reaching the detector could be significantly diminished relative to their prevalence in the collected aerosol. However, the measured ions with a given formula may consist of peroxy-nitrates, di-nitrates, and PAN-like species.

Similar to the highly oxygenated multi-functional species (HOMs) resulting from the ozonolysis of monoterpenes (Ehn et al., 2014; Jokinen et al., 2015), including limonene, many of the observed species could be classified as extremely low-volatility organic compounds (i.e., ELVOC, with the general formula $C_{10}H_{14\text{-}16}O_{7\text{-}11}$), which play a key role in SOA formation (Donahue et al., 2012). Observations performed under ambient conditions during the 2013 Southern Oxidant and Aerosol Study (SOAS) revealed the presence of highly functionalized particulate organic nitrates containing 6–8 oxygen atoms (Lee et al., 2016). In that work, these species constituted 3% and 8% of sub-µm aerosol mass during daytime and nighttime hours, respectively, and exhibited a distinct diurnal pattern, typically reaching peak concentrations between midnight and the early-morning hours. The gaseous parent compounds were identified as monoterpenes, using α-pinene. The similarity with ions from the $NO_3^{\bullet}$-initiated limonene oxidation further emphasizes the importance of monoterpenes as precursors of organic nitrates. Furthermore, the occurrence of such compounds in the ambient environment reinforces the notion that the formation of the highly oxygenated limonene-derived organic nitrate species detected, here, is important to the troposphere.

Through the MCM mechanism, elevated ion signals above *m/z* 390 occurred without formation of the corresponding products. As shown in Fig. 2b, the largest ion signals corresponded to compounds with 19 and 20 carbons in the dimer region. $C_{20}H_{22}N_2O_8$ and $C_{20}H_{29}NO_{17}$, which occurred at significantly elevated levels in all aerosol samples, constituted the lowest- and highest-mass dimers, respectively (see Fig. 2 for other examples of C_{19} and C_{20} dimer species). Many of these can be considered ELVOC species based on their respective formulas (e.g., $C_{19\text{-}20}H_{28\text{-}32}O_{10\text{-}18}$ for dimers) and their partitioning behavior (i.e., they occurred only in the aerosol phase, at levels slightly above background in the gas samples). $C_{19}H_{28}N_2O_x$ and $C_{20}H_{29}NO_x$ were the most dominant families of C_{19} and C_{20} dimers, respectively. Taken together, 10 individual dimers from these two families were identified in all experiments.

The contributions of the 11 most prevalent ion families to the total desorbed organic signal are summarized in Table 2. Average contributions are calculated from the mean signals for each family relative to the total mean organic signal generated during all experiments.

Atmos. Chem. Phys. Discuss., https://doi.org/10.5194/acp-2017-584
Manuscript under review for journal Atmos. Chem. Phys.
Discussion started: 27 June 2017

Atmospheric Chemistry and Physics Discussions

Table 2. Peak desorption temperature (T_{max}) and the average contribution (over all experiments) to the organic signal during SOA desorption for the most commonly observed product families. The number of monomer species in each family that desorbed at only high temperatures is noted in parentheses.

Class	#	Family	# Observed in Family	(N/C)×10	Average Contribution	T_{max} Range (°C)
Monomers	m1	C10H15NOx	5 (1)	1.0	23.0%	74.7 – 152.4
	m2	C10H18N2Ox	2 (0)	2.0	8.8%	66.3 – 69.8
	m3	C10H16N2Ox	5 (1)	2.0	6.7%	51.9 – 154.0
	m4	C10H17NOx	5 (2)	1.0	5.3%	58.7 – 159.2
	m5	C8H11NOx	3 (0)	1.3	4.7%	67.5 – 80.5
	m6	C9H13NOx	4 (0)	1.1	3.0%	70.4 – 74.5
	m7	C9H15NOx	4 (0)	1.1	2.0%	63.9 – 75.7
Dimers	d1	C20H29NOx	4	0.5	7.1%	100.2 – 154.0
	d2	C19H28N2Ox	6	1.1	5.0%	101.1 – 156.9
	d3	C20H27NOx	4	0.5	2.8%	100.5 – 151.3
	d4	C20H24N2Ox	3	1.0	2.0%	124.5 – 156.9

3.2 Characterization of identified ions via thermal properties

The desorption data is characterized by the frequent occurrence of multiple peaks corresponding to certain ions, and the thermograms in all experiments reveal four characteristic desorption patterns, which exhibit the following trends: (i) from 45 to 85°C, some monomer species undergo almost complete desorption. (ii) Some monomers yield two peaks - one in the low-temperature range and another at significantly higher temperatures. Additionally, some monomer ions, associated with certain individual species of the monomer families, occurred at only very high desorption temperatures, owing possibly to the fragmentation of high-mass oligomers and dimers. Although less prominent than that observed for monomers, a double peak occurred for several dimers, whereas for other dimers a single primary desorption peak occurred at mid to high temperatures (110–170°C). The occurrence of multiple peaks is consistent with the thermal degradation of extremely low-volatility species that desorb only at temperatures >200°C. Similar behavior has been observed in previous studies (Holzinger et al., 2010; Lopez-Hilfiker et al., 2014, 2015; Yatavelli et al., 2012), where the secondary peaks observed during desorption were attributed to the thermal degradation of very low-volatility aerosol components.

Analysis of the desorption profiles (thermograms) may yield additional information about the properties of each detected chemical species. The gradual heating of the FIGAERO filter from 25°C to 200°C resulted in a clear volatility-based separation of species and, for each ion detected, the desorption temperature corresponding to the maximum signal was identified. Furthermore, the average desorption temperature of the monomer species was typically lower than that of their dimer counterparts, which are less volatile. Higher masses (than those associated with the monomer species) were typically desorbed from the FIGAERO filter at higher

Atmos. Chem. Phys. Discuss., https://doi.org/10.5194/acp-2017-584
Manuscript under review for journal Atmos. Chem. Phys.
Discussion started: 27 June 2017

Atmospheric Chemistry and Physics Discussions

temperatures. An example of this characteristic behavior is shown in the average thermograms (Fig. 3) of several monomer and dimer ions. In general, compounds evaporating at relatively low temperatures constituted significant fractions of the gas phase, indicative of monomer contributions to the aerosol.

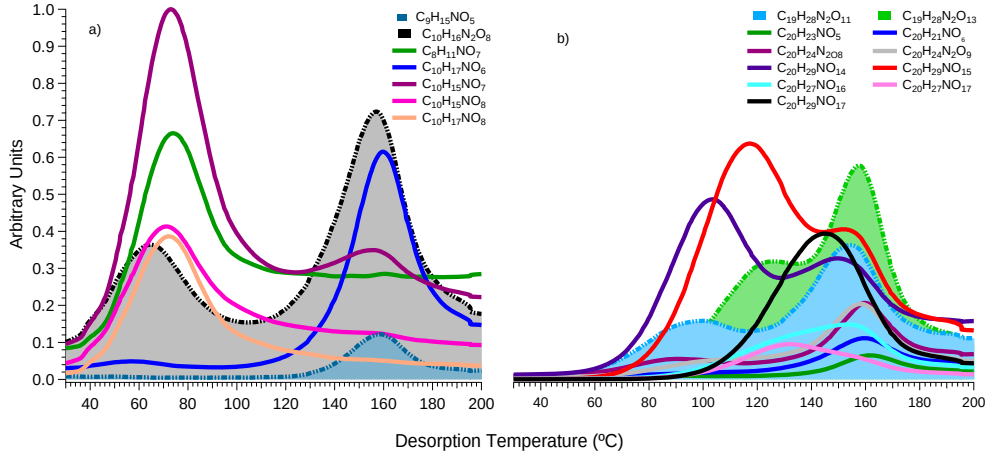

Figure 3. Average thermograms (over four desorption cycles) for an N_2O_5 ratio of 2.4. Thermograms of ion clusters of the (a) monomer species (C_8–C_{10}) and (b) dimer (C_{19}–C_{20}) species. Ions with double-peak thermogram shape patterns, consistent with the fragmentation of low-volatility oligomers, are highlighted.

As shown in Fig. 3, each of the detected ion signals reaches at least one local maximum value. The temperature at which a signal reached the first maximum (T_{max}) value was similar across all experiments (average standard deviation: <10%). Secondary peaks occurred more frequently for species with a carbon number of 10 or lower, consistent with a degradation-based contribution. Although the temperature at which the secondary local maximum occurs ($T_{max,2}$) provides insight into the occurrence of dimerization, the T_{max} value was taken as the true desorption temperature of each ion.

T_{max} values were identified for each ion in the 196-ion set, and (in general) a positive correlation (r^2 = 0.67) was obtained for the dependence of T_{max} on the molecular mass. A few monomer, i.e., lower-mass, species (C ≤ 10) may have formed (via thermal degradation of higher-MW species) mainly as fragments rather than as primary reaction products and, therefore, desorbed only at high temperatures. However, four of these ten species ($C_{10}H_{16}O_4$, $C_{10}H_{17}NO_5$, $C_{10}H_{17}NO_6$, and $C_7H_{10}O_4$) occurred as primary products within the MCM, accounting for (on average) 69.0 ± 10.8% of the signal detected in the gas phase. This suggests that under the investigated N_2O_5 to limonene ratios, dimer formation from these monomer species (which also evaporate as fragments during desorption) is highly favored.

Atmos. Chem. Phys. Discuss., https://doi.org/10.5194/acp-2017-584
Manuscript under review for journal Atmos. Chem. Phys.
Discussion started: 27 June 2017

Atmospheric Chemistry and Physics Discussions

370 The ratio of high-MW species to monomers varied between experiments. At high ratios of
371 N_2O_5 to limonene, the fraction of dimer and oligomer species decreased relative to the total
372 organic signal, whereas the percentage of high-temperature desorbing monomer species
373 (fragments) increased. This suggests that absolute dimer formation may have remained the same,
374 but the monomer signal is over-represented by monomer fragments generated from high-mass,
375 thermally unstable compounds. The average percentages of particle-phase monomers and dimers
376 relative to the ratio of reactants across all experiments are shown in Fig. 4. This percentage is
377 calculated based on the assumption of a common detection sensitivity across all ions; this
378 assumption may influence the estimated (percentage) contribution of monomers relative to that of
379 dimers.

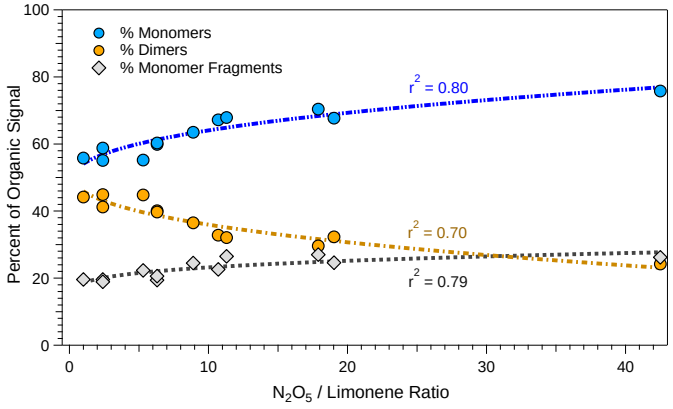

380
381 **Figure 4.** Percentage of monomer, dimer, and high-temperature monomer signal (observed during desorption)
382 relative to the ratio of N_2O_5 to limonene injected into the reactor.

383

384 **3.3 Characterization of major SOA products via cluster analysis**

385 Clustering was performed on an ion set consisting of 117 ions, which accounted for >90%
386 of the total organic signal generated during desorption in all experiments. Ions generating
387 extremely low signal were excluded to prevent analysis of ions with mis-identified T_{max} values.
388 However, the occurrence of high-temperature desorbing monomer outliers (described previously)
389 and the double-peak behavior exhibited by several monomers rendered the mass- and
390 temperature-based grouping of these ions difficult. To address this issue, duplicate entries,
391 corresponding to T_{max} and $T_{max,2}$, were assigned to all ions exhibiting double-peak behavior,
392 allowing the clear separation and analysis of low-mass ions desorbing at temperatures >120°C.

393 Four and five clusters ($\#_{clust}$ = {4, 5}), using T_{max}, MW, and #C as input, yielded the best
394 T_{max}-based clustering and separation of ions. The use of n_H and n_O as additional input parameters
395 resulted in partial separation of clusters into groups with similar O/C and H/C ratios, and poor

Atmos. Chem. Phys. Discuss., https://doi.org/10.5194/acp-2017-584
Manuscript under review for journal Atmos. Chem. Phys.
Discussion started: 27 June 2017

Atmospheric Chemistry and Physics Discussions

correlations with respect to T_{max}. The average silhouette score obtained for four clusters was better (0.81 vs. 0.72) than that obtained for five clusters. However, the use of five clusters allowed for the separation of low-temperature desorbing monomers into two groups with distinct average T_{max}, O/C ratios, and oxidation states. Using more than five clusters resulted in a further decrease in the quality of *cluster separation, as* measured by the inertia (Eq. 1) and average silhouette score (Eq. 2). Although the identification of subgroups within each cluster are possible by increasing $\#_{clust}$, the five main clusters were chosen based on their separation by mass and T_{max} values and to reduce complexity of the interpretation of the resulting clusters with respect to the chemical composition.

Figure 5a shows the cluster separation on the MW–T_{max} plane. The distribution of individual cluster members based on oxidation states and #C (Fig. 5b), and the mean MW, T_{max}, O/C, and oxidation state of each cluster (Fig. 5c) are also shown.

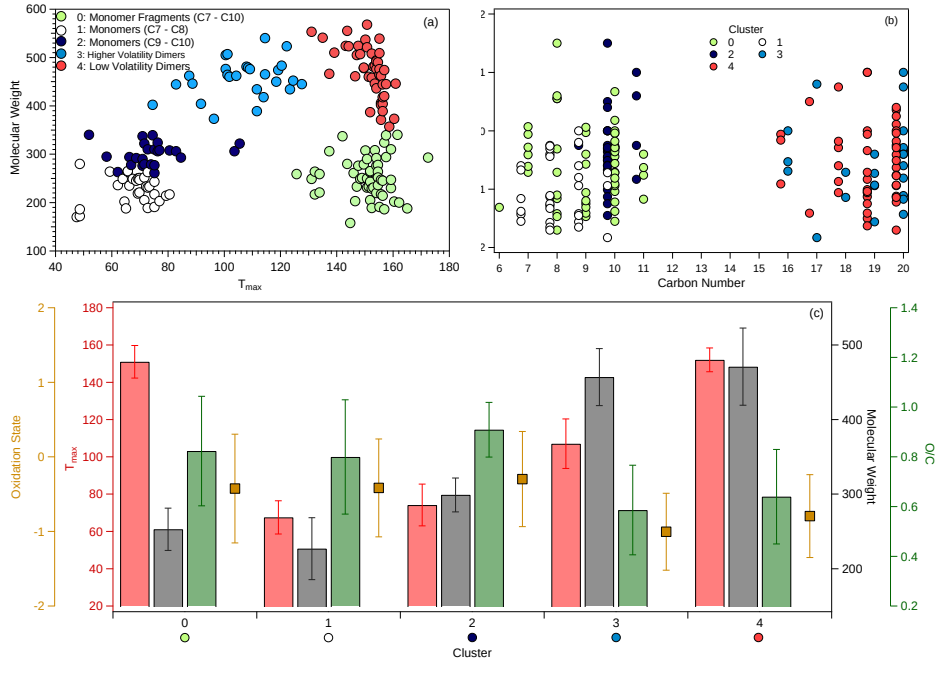

Figure 5. Characteristics of the five identified clusters: (a) Desorption temperature of each observed ion in the top 40th percentile of ions (identified by their respective desorption signal), color-coded by their corresponding cluster number, (b) Oxidation state relative to carbon number of all observed ions, colored by their corresponding cluster membership (for visualization purposes, carbon numbers of groups 0, 2, and 4 are offset), and (c) Average cluster properties with respect to mass, desorption temperature, and oxidation state.

Atmos. Chem. Phys. Discuss., https://doi.org/10.5194/acp-2017-584
Manuscript under review for journal Atmos. Chem. Phys.
Discussion started: 27 June 2017

Atmospheric Chemistry and Physics Discussions

As Fig. 5 shows, the five clusters are characterized by distinct average MWs and corresponding average T_{max} values. Cluster 0 consists of monomer ions, which are considered fragments of larger, less-volatile molecules, that desorb at high temperatures. The average oxidation state and O/C ratio are similar to those of clusters 1 and 2, which are composed primarily of C7–C9 and C9–C10 monomer ions, respectively. This results from the fact that 87% and 69% of cluster 1 and 2 ions, respectively, have secondary thermogram peaks and T_{max} values, and are represented as members of cluster 0. Ions corresponding to the identified dimers are contained in clusters 3 and 4. The dimers are characterized by two primary desorption regimes, with species that desorb at mid-range temperatures (80–130°C) occurring in cluster 3 and the highest-mass, lowest-volatility ions occurring in cluster 4. Moreover, the distribution of individual cluster members with respect to #C and oxidation state (Fig. 5b) shows that members of high-MW clusters (0, 1, 2) and low-MW clusters (3, 4) reside in separate regimes. The ions in high-MW clusters have a significantly larger number of carbon atoms per molecule and, hence, lower (on average) oxidation states than ions in clusters 0–3. With respect to the most prevalent families listed in Table 2, monomer families m2, m3, and m4 reside exclusively in cluster 2, whereas m5 and m7 reside exclusively in cluster 1. Family members of m1 and m6 were split 20/80% and 75/25% between clusters 1 and 2, respectively. Dimer families d1–d4 occurred predominantly (66–75%) in cluster 4, with the remainder residing in cluster 3. None of the dimer families in Table 2 occurred in clusters 0, 1 or 2.

A positive correlation between the average O/C ratios and T_{max} values was obtained for monomer (clusters 1 and 2) and dimer (clusters 3 and 4) groupings, with more highly oxygenated species desorbing at higher temperatures than their less-oxygenated counterparts. This is also reflected in the overall oxidation state of the clusters (2×O/C - H/C - 5×N/C). However, this trend is observed for only a certain range of masses, as lower MW species had (in general) higher O/C ratios than the dimers. This observation provides some insight into the processes of dimerization that are occurring, indicating the extent to which oxygen is lost during the dimerization process.

3.4 Mechanisms of dimerization

Based on the behavior observed in the thermograms for species measured from the limonene SOA in this study, a mechanism of dimer formation, presumably occurring in the particle phase, can be proposed. Dimerization of two monomer species via the loss of one HNO_3 molecule may occur during the processes, and $C_{20}H_{29}NO_y$ (y = 10–18) species would be generated from $C_{10}H_{15}NO_x$ (x = 5–9) species. For example, with HNO_3 as a leaving group, the mechanism of dimerization between $C_{10}H_{15}NO_6$ and $C_{10}H_{15}NO_8$ (see Reaction 3), would produce the C_{20} dimer species ($C_{20}H_{29}NO_{11}$) that was observed in all experiments. The formation of the observed C_{19} dimer species (e.g., $C_{19}H_{27}O_{15}$) through the combination of, for example, $C_{10}H_{17}NO_7$ and $C_9H_{11}NO_{11}$ monomer species (Reaction 4) is also attributed to this mechanism. Additionally, the occurrence of dimer species with two nitrogen atoms, through the combination of monomers such as $C_{10}H_{16}N_2O_9$ and $C_9H_{13}NO_8$ (Reaction 5), can also be attributed to this dimerization mechanism.

Atmos. Chem. Phys. Discuss., https://doi.org/10.5194/acp-2017-584
Manuscript under review for journal Atmos. Chem. Phys.
Discussion started: 27 June 2017

Atmospheric Chemistry and Physics Discussions

$C_{10}H_{15}NO_6 + C_{10}H_{15}NO_8 \rightarrow C_{20}H_{29}NO_{11} + HNO_3$ (R3)

$C_{10}H_{17}NO_7 + C_9H_{11}NO_{11} \rightarrow C_{19}H_{27}NO_{15} + HNO_3$ (R4)

$C_{10}H_{16}N_2O_9 + C_9H_{13}NO_8 \rightarrow C_{19}H_{28}N_2O_{14} + HNO_3$ (R5)

The higher O/C ratios of the monomer species, compared with those of the dimers/oligomers, may also be attributed to the loss of an HNO_3 molecule (from the monomer) during the dimerization process. For example, the two C_{10} reactants in Reaction 3 have O/C ratios of 0.6 and 0.8 while the product, $C_{20}H_{29}NO_{11}$, has an O/C ratio of 0.55. A similar trend is observed for Reactions 4 and 5, where the reactants have an average O/C ratio of 0.96 and 0.89, respectively, and the products have O/C ratios of 0.79 and 0.74, respectively. Due to the loss of HNO_3 during dimerization, dimer fragmentation is expected to yield monomers which differ from the original (i.e., pre-dimerization) monomers. However, the resulting monomers may also be associated with aerosol phase products that have secondary desorption peaks. For example, the fragmentation of $C_{20}H_{29}NO_{11}$ could yield $C_{10}H_{14}O_6 + C_{10}H_{15}NO_5$ or $C_{10}H_{16}O_5 + C_{10}H_{13}NO_6$, and the fragmentation of $C_{19}H_{27}NO_{15}$ might yield $C_9H_{13}NO_6 + C_{10}H_{14}O_9$ or $C_9H_{13}NO_9 + C_{10}H_{14}O_6$. Likewise, $C_9H_{13}NO_7 + C_{10}H_{15}NO_7$ or $C_9H_{13}NO_9 + C_{10}H_{15}NO_5$ monomer pairs could be generated from the thermal degradation of $C_{19}H_{28}N_2O_{14}$.

The fragmentation of dimers may also proceed through multiple channels, thereby producing several sets of monomer fragments, or the fragmentation of multiple dimers may produce the same ions. Therefore, attributing the production of a monomer fragment to the thermal degradation of a specific dimer is difficult, using the current dataset. Large ($C > 20$) oligomeric species may contribute to the high-temperature generation of monomer fragment species. The proposed mechanisms may play only a partial role in the dimerization process occurring in these experiments. However, they offer a plausible explanation for the occurrence of multiple observed dimers and the secondary desorption maxima associated with the monomer constituents.

4 Conclusions

High-resolution mass spectrometric data was obtained for both gas and condensed-phase reaction products resulting from NO_3 initiated oxidation of the monoterpene, limonene. The results revealed that the formation of organic nitrates contributed substantially (89.5 ± 1.4% of the particulate-phase ion signal) to SOA formation, with dimers constituting a significant fraction of the particle-phase products. On average, monomers and dimers/oligomers contributed 62.6 ± 7.2 and 37.4 ± 7.3%, respectively, of the particle-phase organic signal detected by the I-CIMS. Furthermore, many monomers (accounting for 21.6 ± 3.1% of the average organic signal) desorbed at high temperatures (120°C). The fraction of the signal generated by monomers increased with increasing N_2O_5/limonene ratio (ratio of 42.5 yields a fraction of 75.8%), whereas the fraction of dimers decreased (to 24.2%). The fraction of the monomer signal resulting from desorption at high temperatures (≥120ºC) also increased (by 26.2%). Therefore, although the monomer fraction increased with increasing N_2O_5/limonene ratio, this increase in desorption

signal occurred primarily at temperatures above 120ºC, indicative of an increase in the fragmentation of high-MW dimers and oligomers. A large portion (79%) of the monomer thermograms exhibited this bi-modal behavior, with secondary peaks occurring above 120ºC, indicating that the composition of SOA was largely determined by the formation of thermally unstable, low-volatility oligomers.

In total, 196 individual organic ions were detected during desorption. However, the total measured organic signal was generated mainly by 52 (i.e., 76%) of these ions, which constituted the 75th percentile of the monomer and dimer signals. Over half of the signal emanated from the top 90th percentile, which comprised a small subset of only 20 species, of the total number of ions. These 20 species (with nine listed as major products in the MCM) constituted the major particle-phase products formed via the reaction of N_2O_5 and limonene under the conditions employed in this study. The non-listed species were either dimer species or more highly oxygenated, nitrated analogs of known major products, which are notoriously hard to describe via standard gas-phase mechanisms.

Cluster analysis revealed two monomer groups, two dimer groups and, a separate group containing monomer ions that exhibited secondary desorption peaks occurring at temperatures ≥150°C. Each group was characterized by a distinct average MW and desorption temperature (T_{max}). The 2 identified clusters in the monomer and dimer sub-classes differ in oxidation state and O/C ratios, with increasing O/C corresponding to higher T_{max} values. Based on the analysis of these monomer and dimer groups, a mechanism (Reactions 3–5) was proposed for the formation of the observed dimers from the monomers.

Using a combination of cluster analysis and thermal properties derived from Figaero-CIMS measurements may provide some means of reducing the complexity associated with the description of SOA formation processes. The investigated reaction system constitutes only one of many systems, but could be used as an example of the evaluation required for this type of information derived from high-resolution MS. The results revealed that, analogous to products from ozonolysis and $^{\bullet}$OH-induced oxidation, the organic nitrates produced in the nighttime chemistry of biogenic compounds comprise a multi-component mixture that contributes to ambient SOA. Thus, the aerosol species detected here could be included in modeling studies with the aim of explaining scenarios where SOA formation rates are under-predicted. Furthermore, the numerous products resulting from N_2O_5 oxidation of limonene, which were identified and grouped based on thermal properties, could be candidates for identification in ambient air masses dominated by nocturnal limonene chemistry.

Competing interests

The authors declare that they have no conflict of interest.

Acknowledgment

The research presented is a contribution to the Swedish strategic research area ModElling the Regional and Global Earth system, MERGE. This work was supported by the Swedish Research Council (grant numbers 2015-04123; 2014-05332; 2013-06917), Formas (grant number 2015-1537)

References

Arthur, D. and Vassilvitskii, S.: k-means ++: The advantages of careful seeding, ACM-SIAM Symp. Discret. algorithms, 8, 1027–1035, doi:10.1145/1283383.1283494, 2007.

Atkinson, R., Aschmann, S. M., and Pitts, J. N. J.: Rate constants for the gas-phase reactions of the OH radical with a series of monoterpenes at 294 K, Atmos. Environ., 29(17), 2311–2316

Ayres, B. R., Allen, H. M., Draper, D. C., Brown, S. S., Wild, R. J., Jimenez, J. L., Day, D. A., Campuzano-Jost, P., Hu, W., de Gouw, J., Koss, A., Cohen, R. C., Duffey, K. C., Romer, P., Baumann, K., Edgerton, E., Takahama, S., Thornton, J. A., Lee, B. H., Lopez-Hilfiker, F. D., Mohr, C., Goldstein, A. H., Olson, K., and Fry, J. L.: Organic nitrate aerosol formation via NO3 + BVOC in the Southeastern US, Atmos. Chem. Phys. Discuss., 15(12), 16235–16272, doi:10.5194/acpd-15-16235-2015, 2015.

Baptista, L., Pfeifer, R., Da Silva, E. C. and Arbilla, G.: Kinetics and thermodynamics of limonene ozonolysis, J. Phys. Chem. A, 115(40), 10911–10919, doi:10.1021/jp205734h, 2011.

Beaver, M. R., Clair, J. M. St., Paulot, F., Spencer, K. M., Crounse, J. D., LaFranchi, B. W., Min, K. E., Pusede, S. E., Wooldridge, P. J., Schade, G. W., Park, C., Cohen, R. C., and Wennberg, P. O.: Importance of biogenic precursors to the budget of organic nitrates: Observations of multifunctional organic nitrates by CIMS and TD-LIF during BEARPEX 2009, Atmos. Chem. Phys., 12(13), 5773–5785, doi:10.5194/acp-12-5773-2012, 2012.

Bonn, B. and Moorgat, G. K.: New particle formation during α- and β-pinene oxidation by O3, OH and NO3, and the influence of water vapour: Particle size distribution studies, Atmos. Chem. Phys., 2, 183–196, doi:doi:10.5194/acp-2-183-2002, 2002.

Brown, S. S. and Stutz, J.: Nighttime radical observations and chemistry, Chem. Soc. Rev., 41(19), 6405, doi:10.1039/c2cs35181a, 2012.

Bruns, E. A, Perraud, V., Zelenyuk, A., Ezell, M. J., Johnson, S. N., Yu, Y., Imre, D., Finlayson-Pitts, B. J., and Alexander, M. L.: Comparison of FTIR and particle mass spectrometry for the measurement of particulate organic nitrates., Environ. Sci. Technol., 44(3), 1056–1061, doi:10.1021/es9029864, 2010.

Cao, G. and Jang, M.: Secondary organic aerosol formation from toluene photooxidation under various NOx conditions and particle acidity, Atmos. Chem. Phys. Discuss., 8(4), 14467–14495, doi:10.5194/acpd-8-14467-2008, 2008.

564 Carlton, A. G., Wiedinmyer, C., and Kroll, J. H.: A review of secondary organic aerosol (SOA)
565 formation from isoprene, Atmos. Chem. Phys. Discuss., 9(2), 8261–8305, doi:10.5194/acpd-9-
566 8261-2009, 2009.

567 Donahue, N. M., Kroll, J. H., Pandis, S. N., and Robinson, A. L.: A two-dimensional volatility
568 basis set-Part 2: Diagnostics of organic-aerosol evolution, Atmos. Chem. Phys., 12(2), 615–634,
569 doi:10.5194/acp-12-615-2012, 2012.

570 Ehn, M., Thornton, J. A., Kleist, E., Sipilä, M., Junninen, H., Pullinen, I., Springer, M., Rubach,
571 F., Tillmann, R., Lee, B., Lopez-Hilfiker, F., Andres, S., Acir, I.-H., Rissanen, M., Jokinen, T.,
572 Schobesberger, S., Kangasluoma, J., Kontkanen, J., Nieminen, T., Kurtén, T., Nielsen, L. B.,
573 Jørgensen, S., Kjaergaard, H. G., Canagaratna, M., Maso, M. D., Berndt, T., Petäjä, T., Wahner,
574 A., Kerminen, V.-M., Kulmala, M., Worsnop, D. R., Wildt, J., and Mentel, T. F.: A large source
575 of low-volatility secondary organic aerosol, Nature, 506(7489), 476–479,
576 doi:10.1038/nature13032, 2014.

577 Emanuelsson, E. U., Hallquist, M., Kristensen, K., Glasius, M., Bohn, B., Fuchs, H., Kammer,
578 B., Kiendler-Scharr, A., Nehr, S., Rubach, F., Tillmann, R., Wahner, A., Wu, H. C., and Mentel,
579 T. F.: Formation of anthropogenic secondary organic aerosol (SOA) and its influence on biogenic
580 SOA properties, Atmos. Chem. Phys., 13(5), 2837–2855, doi:10.5194/acp-13-2837-2013, 2013.

581 Fry, J. L., Draper, D. C., Barsanti, K. C., Smith, J. N., Ortega, J., Winkler, P. M., Lawler, M. J.,
582 Brown, S. S., Edwards, P. M., Cohen, R. C., and Lee, L.: Secondary organic aerosol formation
583 and organic nitrate yield from NO3 oxidation of biogenic hydrocarbons, Environ. Sci. Technol.,
584 48(3), 11944–11953

585 Fry, J. L., Kiendler-Scharr, A., Rollins, A. W., Brauers, T., Brown, S. S., Dorn, H.-P., Dubé, W.
586 P., Fuchs, H., Mensah, A., Rohrer, F., Tillmann, R., Wahner, A., Wooldridge, P. J., and Cohen,
587 R. C.: SOA from limonene: role of NO3 in its generation and degradation, Atmos. Chem. Phys.,
588 11(8), 3879–3894, doi:10.5194/acp-11-3879-2011, 2011.

589 Fry, J. L., Rollins, A. W., Wooldridge, P. J., Brown, S. S., Fuchs, H., and Dub, W.: Organic
590 nitrate and secondary organic aerosol yield from NO3 oxidation of β-pinene evaluated using a
591 gas-phase kinetics / aerosol partitioning model, Atmos. Chem. Phys., 9(3), 1431–1449,
592 doi:10.5194/acp-9-1431-2009, 2009.

593 Glasius, M. and Goldstein, A. H.: Recent discoveries and future challenges in atmospheric
594 organic chemistry, Environ. Sci. Technol., 50(6), 2754–2764, doi:10.1021/acs.est.5b05105, 2016.

595 Guenther, A. B., Jiang, X., Heald, C. L., Sakulyanontvittaya, T., Duhl, T., Emmons, L. K., and
596 Wang, X.: The model of emissions of gases and aerosols from nature version 2.1 (MEGAN2.1):
597 An extended and updated framework for modeling biogenic emissions, Geosci. Model Dev., 5(6),
598 1471–1492, doi:10.5194/gmd-5-1471-2012, 2012.

599 Guenther, A., Karl, T., Harley, P., Wiedinmyer, C., Palmer, P. I., and Geron, C.: Estimates of
600 global terrestrial isoprene emissions using MEGAN (Model of Emissions of Gases and Aerosols
601 from Nature), Atmos. Chem. Phys., 6(11), 3181–3210, doi:10.5194/acpd-6-107-2006, 2006.

602

603 Guenther, A., Nicholas, C., Erickson, D., Fall, R., Geron, C., Graedel, T., Harley, P., Klinger, L.,
604 Lerdau, M., Mckay, W. A., Pierce, T., Scholes, B., Steinbrecher, R., Tallamraju, R., Taylor, J.,
605 and Zimmerman, P.: A global model of natural volatile organic compound emissions, J. Geophys.
606 Res., 100(94), 8873–8892

607 Hallquist, M., Wängberg, I., Ljungström, E., Barnes, I., and Becker, K. H.: Aerosol and product
608 yields from NO3 radical-initiated oxidation of selected monoterpenes, Environ. Sci. Technol.,
609 33(4), 553–559, doi:10.1021/es980292s, 1999.

610 Hallquist, M., Wenger, J. C., Baltensperger, U., Rudich, Y., Simpson, D., Claeys, M., Dommen,
611 J., Donahue, N. M., George, C., Goldstein, A. H., Hamilton, J. F., Herrmann, H., Hoffmann, T.,
612 Iinuma, Y., Jang, M., Jenkin, M. E., Jimenez, J. L., Kiendler-Scharr, A., Maenhaut, W.,
613 McFiggans, G., Mentel, T. F., Monod, A., Prévôt, A. S. H., Seinfeld, J. H., Surratt, J. D.,
614 Szmigielski, R., and Wildt, J.: The formation, properties and impact of secondary organic
615 aerosol: current and emerging issues, Atmos. Chem. Phys., 9(14), 5155–5236, doi:10.5194/acp-9-
616 5155-2009, 2009.

617 Holzinger, R., Kasper-Giebl, A., Staudinger, M., Schauer, G., and Röckmann, T.: Analysis of the
618 chemical composition of organic aerosol at the Mt. Sonnblick observatory using a novel high
619 mass resolution thermal-desorption proton-transfer-reaction mass-spectrometer (HR-TD-PTR-
620 MS), Atmos. Chem. Phys., 10(20), 10111–10128, doi:10.5194/acp-10-10111-2010, 2010.

621 Jiang, L., Lan, R., Xu, Y. S., Zhang, W. J., and Yang, W.: Reaction of stabilized criegee
622 intermediates from ozonolysis of limonene with water: Ab initio and DFT study, Int. J. Mol. Sci.,
623 14(3), 5784–5805, doi:10.3390/ijms14035784, 2013.

624 Jimenez, J. L., Canagaratna, M. R., Donahue, N. M., Prevot, A. S. H., Zhang, Q., Kroll, J. H.,
625 Decarlo, P. F., Allan, J. D., Coe, H., Ng, N. L., Aiken, A. C., Ulbrich, I. M., Grieshop, A. P.,
626 Duplissy, J., Wilson, K. R., Lanz, V. A., Hueglin, C., Sun, Y. L., Tian, J., Laaksonen, A.,
627 Raatikainen, T., Rautiainen, J., Vaattovaara, P., Ehn, M., Kulmala, M., Tomlinson, J. M.,
628 Cubison, M. J., Dunlea, E. J., Alfarra, M. R., Williams, P. I., Bower, K., Kondo, Y., Schneider,
629 J., Drewnick, F., Borrmann, S., Weimer, S., Demerjian, K., Salcedo, D., Cottrell, L., Takami, A.,
630 Miyoshi, T., Shimono, A., Sun, J. Y., Zhang, Y. M., Dzepina, K., Sueper, D., Jayne, J. T.,
631 Herndon, S. C., Williams, L. R., Wood, E. C., Middlebrook, A. M., Kolb, C. E., Baltensperger,
632 U., and Worsnop, D. R.: Evolution of organic aerosols in the atmosphere, Science 326, 1525–
633 1529

634 Jokinen, T., Berndt, T., Makkonen, R., Kerminen, V.-M., Junninen, H., Paasonen, P., Stratmann,
635 F., Herrmann, H., Guenther, A. B., Worsnop, D. R., Kulmala, M., Ehn, M., and Sipilä, M.:
636 Production of extremely low volatile organic compounds from biogenic emissions: Measured
637 yields and atmospheric implications., Proc. Natl. Acad. Sci. U. S. A., 112(23), 7123–7128,
638 doi:10.1073/pnas.1423977112, 2015.

639 Jonsson, Å. M., Hallquist, M., and Ljungström, E.: Impact of humidity on the ozone initiated
640 oxidation of limonene, Δ3-carene, and α-pinene, Environ. Sci. Technol., 40(1), 188–194,
641 doi:10.1021/es051163w, 2006.

642

643 Jonsson, Å. M., Hallquist, M., and Ljungström, E.: The effect of temperature and water on
644 secondary organic aerosol formation from ozonolysis of limonene, Δ3-carene and α-pinene,
645 Atmos. Chem. Phys., 8(21), 6541–6549, doi:10.5194/acp-8-6541-2008, 2008a.

646 Jonsson, Å. S. A. M., Hallquist, M., Ljungstro, E., Jonsson, Å. S. A. M., and Hallquist, M.:
647 Influence of OH scavenger on the water effect on secondary organic influence of OH scavenger
648 on the water effect on secondary organic aerosol formation from ozonolysis of limonene , Δ3-
649 carene, and α-pinene, Environ. Sci. Technol., 42(16), 5938–5944, doi:10.1021/es702508y, 2008b.

650 Kanakidou, M., Seinfeld, J. H., Pandis, S. N., Barnes, I., Dentener, F. J., Facchini, M. C., Van
651 Dingenen, R., Ervens, B., Nenes, A., Nielsen, C. J., Swietlicki, E., Putaud, J. P., Balkanski, Y.,
652 Fuzzi, S., Horth, J., Moortgat, G. K., Winterhalter, R., Myhre, C. E. L., Tsigaridis, K., Vignati,
653 E., Stephanou, E. G., and Wilson, J.: Organic aerosol and global climate modelling: A review,
654 Atmos. Chem. Phys., 5(4), 1053–1123, doi:10.5194/acp-5-1053-2005, 2005.

655 Kourtchev, I., Fuller, S. J., Giorio, C., Healy, R. M., Wilson, E., O'Connor, I., Wenger, J. C.,
656 McLeod, M., Aalto, J., Ruuskanen, T. M., Maenhaut, W., Jones, R., Venables, D. S., Sodeau, J.
657 R., Kulmala, M., and Kalberer, M.: Molecular composition of biogenic secondary organic
658 aerosols using ultrahigh-resolution mass spectrometry: Comparing laboratory and field studies,
659 Atmos. Chem. Phys., 14(4), 2155–2167, doi:10.5194/acp-14-2155-2014, 2014.

660 Kourtchev, I., Giorio, C., Manninen, A., Wilson, E., Mahon, B., Aalto, J., Kajos, M., Venables,
661 D., Ruuskanen, T., Levula, J., Loponen, M., Connors, S., Harris, N., Zhao, D., Kiendler-Scharr,
662 A., Mentel, T., Rudich, Y., Hallquist, M., Doussin, J.-F., Maenhaut, W., Bäck, J., Petäjä, T.,
663 Wenger, J., Kulmala, M., and Kalberer, M.: Enhanced Volatile Organic Compounds emissions
664 and organic aerosol mass increase the oligomer content of atmospheric aerosols, Nat. Sci.
665 Reports, 6(September), 35038, doi:10.1038/srep35038, 2016.

666 Kristensen, K., Watne, Å. K., Hammes, J., Lutz, A., Petäjä, T., Hallquist, M., Bilde, M., and
667 Glasius, M.: High-molecular weight dimer esters are major products in aerosols from α-pinene
668 ozonolysis and the Boreal forest, Environ. Sci. Technol. Lett., 3(8), 280–285,
669 doi:10.1021/acs.estlett.6b00152, 2016.

670 Kroll, J. H., Chan, A. W. H., Ng, N. G. A. L., and Flagan, R. C.: Reactions of semivolatile
671 organics and their Effects on secondary organic aerosol formation, Environ. Sci. Technol.,
672 41(10), 3545–3550

673 Kroll, J. H. and Seinfeld, J. H.: Chemistry of secondary organic aerosol: Formation and evolution
674 of low-volatility organics in the atmosphere, Atmos. Environ., 42(16), 3593–3624,
675 doi:10.1016/j.atmosenv.2008.01.003, 2008.

676 Lee, B. H., Lopez-Hilfiker, F. D., Mohr, C., Kurtén, T., Worsnop, D. R., and Thornton, J. A.: An
677 iodide-adduct high-resolution time-of-flight chemical-ionization mass spectrometer: Application
678 to atmospheric inorganic and organic compounds., Environ. Sci. Technol., 48(11), 6309–6317,
679 doi:10.1021/es500362a, 2014a.

680

Lee, B. H., Mohr, C., Lopez-Hilfiker, F. D., Lutz, A., Hallquist, M., Lee, L., Romer, P., Cohen, R. C., Iyer, S., Kurten, T., Hu, W., Day, D. A., Campuzano-Jost, P., Jimenez, J. L., Xu, L., Ng, N. L., Guo, H., Weber, R. J., Wild, R. J., Brown, S. S., Koss, A., de Gouw, J., Olson, K., Goldstein, A. H., Seco, R., Kim, S., McAvey, K., Shepson, P. B., Starn, T., Baumann, K., Edgerton, E. S., Liu, J., Shilling, J. E., Miller, D. O., Brune, W., Schobesberger, S., D'Ambro, E. L., and Thornton, J. A.: Highly functionalized organic nitrates in the southeast United States: Contribution to secondary organic aerosol and reactive nitrogen budgets, Proc. Natl. Acad. Sci. U. S. A., 113(6), 1516–1521, doi:10.1073/pnas.1508108113, 2016.

Lee, L., Wooldridge, P. J., Gilman, J. B., Warneke, C., de Gouw, J., and Cohen, R. C.: Low temperatures enhance organic nitrate formation: Evidence from observations in the 2012 Uintah Basin Winter Ozone Study, Atmos. Chem. Phys., 14(22), 12441–12454, doi:10.5194/acp-14-12441-2014, 2014b.

Leungsakul, S., Jaoui, M., and Kamens, R. M.: Kinetic mechanism for predicting secondary organic aerosol formation from the reaction of d-limonene with ozone., Environ. Sci. Technol., 39(24), 9583–9594, doi:10.1021/es0492687, 2005.

Lopez-Hilfiker, F. D., Mohr, C., Ehn, M., Rubach, F., Kleist, E., Wildt, J., Mentel, T. F., Carrasquillo, A., Daumit, K., Hunter, J., Kroll, J. H., Worsnop, D., and Thornton, J. A.: Phase partitioning and volatility of secondary organic aerosol components formed from α-pinene ozonolysis and OH oxidation: The importance of accretion products and other low volatility compounds, Atmos. Chem. Phys. Discuss., 15, 4463–4494, doi:10.5194/acpd-15-4463-2015, 2015.

Lopez-Hilfiker, F. D., Mohr, C., Ehn, M., Rubach, F., Kleist, E., Wildt, J., Mentel, T. F., Lutz, A., Hallquist, M., Worsnop, D., and Thornton, J. A.: A novel method for online analysis of gas and particle composition: Description and evaluation of a Filter Inlet for Gases and AEROsols (FIGAERO), Atmos. Meas. Tech., 7(4), 983–1001, doi:DOI 10.5194/amt-7-983-2014, 2014.

McKinney, W.: Data structures for statistical computing in Python, Proc. 9th Python Sci. Conf., 1697900(Scipy), 51–56 [online] Available from: http://conference.scipy.org/proceedings/scipy2010/mckinney.html, 2010.

McKinney, W.: pandas: A foundational Python library for data analysis and statistics, Python High Perform. Sci. Comput., 1–9

Mentel, T. F., Springer, M., Ehn, M., Kleist, E., Pullinen, I., Kurtén, T., Rissanen, M., Wahner, A., and Wildt, J.: Formation of highly oxidized multifunctional compounds: Autoxidation of peroxy radicals formed in the ozonolysis of alkenes – deduced from structure–product relationships, Atmos. Chem. Phys., 15(12), 6745–6765, doi:10.5194/acp-15-6745-2015, 2015.

Müller, L., Reinnig, M.-C., Warnke, J., and Hoffmann, T.: Unambiguous identification of esters as oligomers in secondary organic aerosol formed from cyclohexene and cyclohexene/α-pinene ozonolysis, Atmos. Chem. Phys. Discuss., 7, 13883–13913, doi:10.5194/acpd-7-13883-2007, 2007.

720 Murphy, B. N., Donahue, N. M., Robinson, A. L., and Pandis, S. N.: A naming convention for
721 atmospheric organic aerosol, Atmos. Chem. Phys., 14(11), 5825–5839, doi:10.5194/acp-14-5825-
722 2014, 2014.

723 Myhre, G., Shindell, D., Bréon, F.-M., Collins, W., Fuglestvedt, J., Huang, J., Koch, D.,
724 Lamarque, J.-F., Lee, D., Mendoza, B., Nakajima, T., Robock, A., Stephens, G., Takemura, T.,
725 and Zhan, H.: Anthropogenic and natural radiative forcing: In Climate Change 2013: The
726 Physical Science Basis. Contribution of Working Group I to the Fifth Assessment Report of the
727 Intergovernmental Panel on Climate Change, Cambridge Univ. Press. Cambridge, United
728 Kingdom New York, NY, USA, 659–740, doi:10.1017/ CBO9781107415324.018, 2013.

729 Orlando, J. J., Tyndall, G. S., and Calvert, J. G.: Thermal decomposition pathways for
730 peroxyacetyl nitrate (PAN): Implications for atmospheric methyl nitrate levels, Atmos. Environ.
731 Part A, Gen. Top., 26(17), 3111–3118, doi:10.1016/0960-1686(92)90468-Z, 1992.

732 Pathak, R. K., Salo, K., Emanuelsson, E. U., Cai, C., Lutz, A., Hallquist, Å. M., and Hallquist,
733 M.: Influence of ozone and radical chemistry on limonene organic aerosol production and
734 thermal characteristics, Environ. Sci. Technol., 46, 11660–11669

735 Paulot, F., Crounse, J. D., Kjaergaard, H. G., Kroll, J. H., Seinfeld, J. H., and Wennberg, P. O.:
736 Isoprene photooxidation: New insights into the production of acids and organic nitrates, Atmos.
737 Chem. Phys., 9(4), 1479–1501, doi:10.5194/acp-9-1479-2009, 2009.

738 Pedregosa, F., Grisel, O., Weiss, R., Passos, A., and Brucher, M.: Scikit-learn: Machine learning
739 in Python, J. Mach. Learn. Res., 12, 2825–2830, doi:10.1007/s13398-014-0173-7.2, 2011.

740 Perraud, V., Bruns, E. A, Ezell, M. J., Johnson, S. N., Greaves, J., and Finlayson-Pitts, B. J.:
741 Identification of organic nitrates in the NO3 radical initiated oxidation of alpha-pinene by
742 atmospheric pressure chemical ionization mass spectrometry., Environ. Sci. Technol., 44(15),
743 5887–93, doi:10.1021/es1005658, 2010.

744 Perring, A. E., Bertram, T. H., Wooldridge, P. J., Fried, A., Heikes, B. G., Dibb, J., Crounse, J.
745 D., Wennberg, P. O., Blake, N. J., Blake, D. R., Brune, W. H., Singh, H. B., and Cohen, R. C.:
746 Airborne observations of total RONO2: New constraints on the yield and lifetime of isoprene
747 nitrates, Atmos. Chem. Phys., 9(4), 1451–1463, doi:10.5194/acp-9-1451-2009, 2009.

748 Perring, A. E., Pusede, S. E., and Cohen, R. C.: An observational perspective on the atmospheric
749 impacts of alkyl and multifunctional nitrates on ozone and secondary organic aerosol, Chem.
750 Rev.

751 Presto, A. A., Hartz, K. E. H., and Donahue, N. M.: Secondary organic aerosol production from
752 terpene ozonolysis. 1. Effect of UV radiation., Environ. Sci. Technol., 39(18), 7036–7045,
753 doi:10.1021/es050174m, 2005a.

754 Presto, A. A., Hartz, K. E. H., Donahue, N. M., Huff Hartz, K. E., Donahue, N. M., Hartz, K. E.
755 H., Donahue, N. M., Huff Hartz, K. E., and Donahue, N. M.: Secondary organic aerosol
756 production from terpene ozonolysis. 2. Effect of NOx concentration, Environ. Sci. Technol.,
757 39(18), 7046–7054, doi:10.1021/es050400s, 2005b.

758

759 Raschka, S.: Python machine learning, edited by A. Hussain, Packt Publishin Ltd., Birmingham,
760 UK. [online] Available from: www.packtpub.com, 2016.

761 Rindelaub, J. D., Mcavey, K. M., and Shepson, P. B.: The photochemical production of organic
762 nitrates from α-pinene and loss via acid-dependent particle phase hydrolysis, Atmos. Environ.,
763 100, 193–201, doi:10.1016/j.atmosenv.2014.11.010, 2015.

764 Rindelaub, J. D., McAvey, K. M., and Shepson, P. B.: Determination of α-pinene-derived organic
765 nitrate yields: Particle phase partitioning and hydrolysis, Atmos. Chem. Phys. Discussions., 2014.

766 Roberts, J. M.: Chemistry of organic nitrates, Atmos. Environ., 24(2), 243–287

767 Rollins, A. W., Browne, E. C., Pusede, S. E., Wooldridge, P. J., Gentner, D. R., Goldstein, A. H.,
768 Liu, S., Day, D. A., and Cohen, R. C.: Evidence for NOx control over nighttime SOA formation,
769 Science, 267(September), 1210–1212

770 Rollins, A. W., Pusede, S., Wooldridge, P., Min, K.-E., Gentner, D. R., Goldstein, A. H., Liu,
771 S., Day, D. A., Russell, L. M., Rubitschun, C. L., Surratt, J. D., and Cohen, R. C.: Gas/particle
772 partitioning of total alkyl nitrates observed with TD-LIF in Bakersfield, J. Geophys. Res. Atmos.,
773 118(12), 6651–6662, doi:10.1002/jgrd.50522, 2013.

774 Rousseeuw, P. J.: Silhouettes: A graphical aid to the interpretation and validation of cluster
775 analysis, J. Comput. Appl. Math., 20(C), 53–65, doi:10.1016/0377-0427(87)90125-7, 1987.

776 Saunders, S. M., Jenkin, M. E., Derwent, R. G., and Pilling, M. J.: Protocol for the development
777 of the Master Chemical Mechanism, MCM v3 (Part A): Tropospheric degradation of non-
778 aromatic volatile organic compounds, Atmos. Chem. Phys., 3(1), 161–180, doi:10.5194/acp-3-
779 161-2003, 2003.

780 Singh, H. B. and Hanst, P. L.: Peroxyacetyl nitrate (PAN) in the unpolluted atmosphere: An
781 important reservoir for nitrogen oxides, Geopys. Res. Lett., 8(8), 941–944

782 Smith, J. N., Dunn, M. J., VanReken, T. M., Iida, K., Stolzenburg, M. R., McMurry, P. H., and
783 Huey, L. G.: Chemical composition of atmospheric nanoparticles formed from nucleation in
784 Tecamac, Mexico: Evidence for an important role for organic species in nanoparticle growth,
785 Geophys. Res. Lett., 35(4), 2–6, doi:10.1029/2007GL032523, 2008.

786 Spittler, M., Barnes, I., Bejan, I., Brockmann, K. J. J., Benter, T., and Wirtz, K.: Reactions of
787 NO3 radicals with limonene and α-pinene: Product and SOA formation, Atmos. Environ., 40(3),
788 116–127, doi:10.1016/j.atmosenv.2005.09.093, 2006.

789 Sun, T., Wang, Y., Zhang, C., Sun, X., and Wang, W.: The chemical mechanism of the limonene
790 ozonolysis reaction in the SOA formation: A quantum chemistry and direct dynamic study,
791 Atmos. Environ., 45(9), 1725–1731, doi:10.1016/j.atmosenv.2010.12.054, 2011.

792 Temple, P. J. and Taylor, O. C.: World-wide ambient measurements of peroxyacetyl nitrate
793 (PAN) and implications for plant injury, Atmos. Environ., 17(8), 1583–1587, doi:10.1016/0004-
794 6981(83)90311-6, 1983.

795

796 Tolocka, M. P., Jang, M., Ginter, J. M., Cox, F. J., Kamens, R. M., and Johnston, M. V.:
797 Formation of oligomers in secondary organic aerosol, Environ. Sci. Technol., 38(5), 1428–1434,
798 doi:10.1021/es035030r, 2004.

799 Tuazon, E. C., Carter, W. P. L., and Atkinson, R.: Thermal decomposition of peroxyacetyl nitrate
800 and reactions of acetyl peroxy radicals with NO and NO2 over the temperature range 283–313 K,
801 J. Phys. Chem., 95, 2434–2437

802 Wainman, T., Zhang, J., Weschler, C. J., and Lioy, P. J.: Ozone and limonene in indoor air: A
803 source of submicron particle exposure, Environ. Health Perspect., 108(12), 1139–1145,
804 doi:10.1289/ehp.001081139, 2000.

805 Van Der Walt, S., Colbert, S. C., and Varoquaux, G.: The NumPy array: A structure for efficient
806 numerical computation, Comput. Sci. Eng., 13(2), 22–30, doi:10.1109/MCSE.2011.37, 2011.

807 Wehner, B., Petäjä, T., Boy, M., Engler, C., Birmili, W., Tuch, T., Wiedensohler, A., and
808 Kulmala, M.: The contribution of sulfuric acid and non-volatile compounds on the growth of
809 freshly formed particles at Melpitz, Geophys. Res. Lett., 32(L17810), doi:10.1063/1.4803246,
810 2005.

811 Wooldridge, P. J., Perring, A. E., Bertram, T. H., Flocke, F. M., Roberts, J. M., Singh, H. B.,
812 Huey, L. G., Thornton, J. A., Wolfe, G. M., Murphy, J. G., Fry, J. L., Rollins, A. W., Lafranchi,
813 B. W., and Cohen, R. C.: Total Peroxy Nitrates (ΣPNs) in the atmosphere: The Thermal
814 Dissociation-Laser Induced Fluorescence (TD-LIF) technique and comparisons to speciated PAN
815 measurements, Atmos. Meas. Tech., 3(3), 593–607, doi:10.5194/amt-3-593-2010, 2010.

816 Yatavelli, R. L. N., Lopez-Hilfiker, F., Wargo, J. D., Kimmel, J. R., Cubison, M. J., Bertram, T.
817 H., Jimenez, J. L., Gonin, M., Worsnop, D. R., and Thornton, J. A.: A Chemical Ionization High-
818 Resolution Time-of-Flight Mass Spectrometer Coupled to a Micro Orifice Volatilization
819 Impactor (MOVI-HRToF-CIMS) for analysis of gas and particle-phase organic species, Aerosol
820 Sci. Technol., 46(12), 1313–1327, doi:10.1080/02786826.2012.712236, 2012.

821 Youssefi, S. and Waring, M. S.: Transient secondary organic aerosol formation from d-limonene
822 and a-pinene ozonolysis in indoor environments, Indoor Air 2014 - 13th Int. Conf. Indoor Air
823 Qual. Clim., 145–152 [online] Available from: http://www.scopus.com/inward/record.url?eid=2-
824 s2.0-84924705682&partnerID=tZOtx3y1, 2014.

825 Zhang, J., Hartz, K. E. H., Pathak, R. K., Pandis, S. N., and Donahue, N. M.: Secondary organic
826 aerosol formation from limonene ozonolysis: NOx and ultraviolet effects, J. Phys. Chem. A,
827 110(38), 11053–11063

828 Ziemann, P. J. and Atkinson, R.: Kinetics, products, and mechanisms of secondary organic
829 aerosol formation, Chem. Soc. Rev., 41(19), 6582, doi:10.1039/c2cs35122f, 2012.

830